Article

In Vivo Magnetic Resonance Detection of Cancer by Using Multifunctional Magnetic Nanocrystals

Yong-Min Huh, Young-wook Jun, Ho-Taek Song, Sungjun Kim, Jin-sil Choi, Jae-Hyun Lee, Sarah Yoon, Kyung-Sup Kim, Jeon-Soo Shin, Jin-Suck Suh, and Jinwoo Cheon

J. Am. Chem. Soc., **2005**, 127 (35), 12387-12391• DOI: 10.1021/ja052337c • Publication Date (Web): 16 August 2005

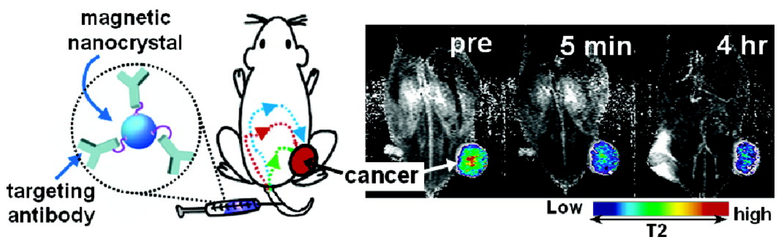

J|A|C|S
ARTICLES
Published on Web 08/16/2005

In Vivo Magnetic Resonance Detection of Cancer by Using Multifunctional Magnetic Nanocrystals

Yong-Min Huh,[†,‡] Young-wook Jun,[†,§] Ho-Taek Song,[†,‡] Sungjun Kim,[†,‡] Jin-sil Choi,[†,§] Jae-Hyun Lee,[†,§] Sarah Yoon,[¶] Kyung-Sup Kim,[¶] Jeon-Soo Shin,[†,¶] Jin-Suck Suh,*[,†,‡] and Jinwoo Cheon*[,†,§]

Contribution from the Yonsei Nano-Medical Core Research Center, Department of Radiology, Department of Chemistry, Department of Biochemistry and Molecular Biology, and Department of Microbiology, Yonsei University, Seoul 120-752, Korea

Received April 11, 2005; E-mail: jss@yumc.yonsei.ac.kr; jcheon@yonsei.ac.kr

Abstract: The unique properties of magnetic nanocrystals provide them with high potential as key probes and vectors in the next generation of biomedical applications. Although superparamagnetic iron oxide nanocrystals have been extensively studied as excellent magnetic resonance imaging (MRI) probes for various cell trafficking, gene expression, and cancer diagnosis, further development of in vivo MRI applications has been very limited. Here, we describe in vivo diagnosis of cancer, utilizing a well-defined magnetic nanocrystal probe system with multiple capabilities, such as small size, strong magnetism, high biocompatibility, and the possession of active functionality for desired receptors. Our magnetic nanocrystals are conjugated to a cancer-targeting antibody, Herceptin, and subsequent utilization of these conjugates as MRI probes has been successfully demonstrated for the monitoring of in vivo selective targeting events of human cancer cells implanted in live mice. Further conjugation of these nanocrystal probes with fluorescent dye-labeled antibodies enables both in vitro and ex vivo optical detection of cancer as well as in vivo MRI, which are potentially applicable for an advanced multimodal detection system. Our study finds that high performance in vivo MR diagnosis of cancer is achievable by utilizing improved and multifunctional material properties of iron oxide nanocrystal probes.

Colloidal nanocrystals have potential to bring dramatic improvements to biomedical sciences, including detection, diagnosis, and therapeutic systems.[1,2] In addition to their small sizes, comparable to biological functional molecules, the ability to tune the nanocrystalline properties through controlling their size, shape, and composition makes these materials useful and optimized for the biomedical purposes. These nanocrystals exhibit remarkably enhanced optical, magnetic, and electronic properties compared to that of their bulk counterparts.[3−5] These properties of nanocrystals can lead to the development of a new tool to detect and control biologically active processes at the molecular and cellular level. Among these nanocrystals, semiconductor quantum dots have been demonstrated as excellent fluorescent probes for imaging,[6−8] signaling,[9] evolution,[10] and targeting[11] of cells. When it comes to their in vivo clinical applications in live animals, however, except in some cases,[10−12] quantum dots suffer from the intrinsic limitations of optical systems, such as low penetration depth of light through tissues and large background fluorescence.

While they have received much less attention than quantum dots, magnetic nanocrystals are now emerging in biomedical applications with new possibilities while circumventing the limitations of optical systems. In particular, magnetic nanocrystals can be utilized as magnetic probes with signal-enhancing capability, which can resolve the weakness of current MRI techniques. Although MRI has been one of the most powerful medical diagnostic tools, due to its noninvasive nature and multidimensional tomographic capabilities coupled with high spatial resolution, its low-signal sensitivity has been a problem. Clinically benign iron-oxide-based magnetic nanoparticles (e.g., superparamagnetic iron oxide (SPIO) and its related systems) have been widely explored for such signal-enhancing purposes. Magnetic labeling of cells,[13,14] in vitro molecular labeling of

† Yonsei Nano-Medical Core Research.
‡ Department of Radiology.
§ Department of Chemistry.
¶ Department of Biochemistry and Molecular Biology.

(1) Alivisatos, A. P. *Nat. Biotechnol.* **2004**, *22*, 47−51.
(2) Elgahanian, R.; Storfoff, J. J.; Mucic, R. C.; Lestinger, R. L.; Mirkin, C. A. *Science* **1997**, *277*, 1078−1081.
(3) Murray, C. B.; Norris, D. J.; Bawendi, M. G. *J. Am. Chem. Soc.* **1993**, *115*, 8706−8715.
(4) Alivisatos, A. P. *Science* **1996**, *271*, 933−937.
(5) Zeng, H.; Li, J.; Liu, J. P.; Wang, Z. L.; Sun, S. *Nature* **2002**, *420*, 395−398.
(6) Bruchez, M.; Moronne, M.; Gin, P.; Weiss, S.; Alivisatos, A. P. *Science* **1998**, *281*, 2013−2016.
(7) Chan, W. C. W.; Nie, S. *Science* **1998**, *281*, 2016−2018.
(8) Wu, X. Y.; Liu, H. J.; Liu, J. Q.; Haley, K. N.; Treadway, J. A.; Larson, J. P.; Ge, N. F.; Peale, F.; Bruchez, M. P. *Nat. Biotechnol.* **2003**, *21*, 41−46.
(9) Lidke, D. S.; Nagy, P.; Heintzmann, R.; Arndt-Jovin, D. J.; Post, J. N.; Grecco, H. E.; Jares-Erijman, E. A.; Jovin, T. M. *Nat. Biotechnol.* **2004**, *22*, 198−203.
(10) Dubertret, B.; Skourides, P.; Norris, D. J.; Noireaux, V.; Brivanlou, A. H.; Libchaber, A. *Science* **2002**, *298*, 1759−1762.
(11) Gao, X.; Cui, Y.; Levenson, R. M.; Chung, L. W. K.; Nie, S. *Nat. Biotechnol.* **2004**, *22*, 969−976.
(12) Kim, S. et al. *Nat. Biotechnol.* **2004**, *22*, 93−97.

E-Selectin in endothelial cells by using SPIO−antibody conjugates,[15] and in vitro MR imaging of the HER2/*neu* receptor by using avidin−SPIO and the biotinylated Herceptin targeting system[16] are some of the important advances. Their utilizations have been, however, mostly limited to in vitro systems with very few successful demonstrations in the in vivo systems.[17,18] Some of the main difficulties of in vivo MRI lie in lack of high-quality biocompatible magnetic nanocrystals. Therefore, one of the current challenges is to develop well-defined magnetic nanocrystals with multiple capabilities, such as optimal nanoscale magnetism, high biostability, which withstands harsh biological conditions (e.g., variable pH, salt concentration), the ability to escape from the reticuloendothelial system (RES), and the possession of active functionality, such as a targeting moiety for desired receptors.

Very recently, we have reported water-soluble magnetic iron oxide (abbreviated as WSIO) nanocrystals with tunable MR signal-enhancing effect by systematically controlling the nanocrystal size.[19] In addition, our previous study showed the preliminary in vitro MR probe results for the diagnosis of a specific breast cancer cell line (SK-BR-3). In this report, we now present the successful in vivo diagnosis of breast cancer in live mice by using the magnetic nanocrystal−antibody probe system. We also report the comprehensive and thorough MR signal-enhancing effects of various cell lines with different levels of cancer marker expressions and also of different magnetic fields (1.5 and 9.4 T). At a high magnetic field of 9.4 T, our probe system enables the detailed monitoring of dynamic targeting events of cancer cells, which reveal complex vasculature structures of the tumor tissue. Along with such MR studies, independent optical detection of cancer has been performed to confirm our MRI results by staining the nanocrystal−antibody probe conjugates with dye-labeled secondary antibody of human IgG.

Experimental Section

Materials. All chemicals were purchased from Aldrich and Sigma. Sephacryl S-300 was purchased from Amersham Biosciences. Iron oxide nanocrystals were synthesized from modified procedures reported previously.[20] Herceptin was purchased from Roche Pharma Ltd. Fluorescein (FITC)-labeled anti-human IgG was purchased from ICN (Ohio). Rat anti-CD31 IgG and rhodamine-labeled anti-rat IgG were purchased from abcam (Cambridge, UK). All cell lines including hepatoma cell lines (Bx-PC-3), breast cancer cell lines (MDA-MB-231, BT474), and fibroblast cell lines (NIH3T6.7) were purchased from American Type Culture Collection (ATCC). Cross-linked iron oxide (CLIO) was a generous gift from Dr. G. G. Cho (KBSI).

Phase Transfer of Fe_3O_4 Nanocrystals from the Organic to the Aqueous Phase. The phase transfer reaction was performed through the reaction of as-synthesized iron oxide nanocrystals with a large excess of 2,3-dimercaptosuccinic acid (DMSA), following our previous report.[19] In a typical experiment, Fe_3O_4 nanocrystals (∼10 mg) with desired sizes were dissolved in 1 mL of toluene. 2,3-Dimercaptosuccinic acid molecules (∼5 mg) were dissolved in 1 mL of dimethyl sulfoxide (DMSO), and the solution is added into the nanocrystal solution. The resulting solution was vortexed for 24 h, and black precipitates were observed, which were isolated through centrifugation and dissolved in water. To remove some portion of aggregated particles, the nanocrystal solution was filtered through a 0.2 μm syringe filter. Purification of the nanocrystal solution was performed through gel filtration with Sephadex G-25.

Conjugation of Water-Soluble Iron Oxide Nanocrystals with Herceptin. Four milligrams of Herceptin was dissolved in 400 μL of 10 mM phosphate-buffered solution (pH 7.2) and mixed with 0.2 mg of sulfo-SMCC. After 30 min, the maleimide-activated Herceptin was purified by applying the reaction mixture to a desalting column packed with Sephadex G-25. The purified Herceptin was added to 100 μL of a water-soluble iron oxide nanocrystal solution (2 mg/mL) and reacted for 4 h at room temperature. The iron oxide−Herceptin conjugates were isolated from the reaction solution by gel filtration with Sephacryl S-300.

In Vitro and In Vivo Mouse MR Imaging. MR imaging was performed with a 1.5 T clinical MRI instrument with a micro-47 surface coil (Intera; Philips Medical Systems, Best, The Netherlands) or with a 9.4 T research magnet (Biospin; Bruker, Germany). For T2-weighted MR imaging of in vitro cells at 1.5 T, the following parameters were adopted: point resolution = 156 × 156 μm, section thickness = 0.6 mm, TE = 60 ms, TR = 4000 ms, number of acquisitions = 1. For T2 mapping of a live mouse at 1.5 T, the following parameters were adopted: point resolution = 234 × 234 μm, section thickness = 3.0 mm, TE = 20, 40, 60, 80, 100, 120, 140, and 160 ms, TR = 4000 ms, number of acquisitions = 2. For T2*-weighted MR imaging of a live mouse at 9.4 T, the following parameters were adopted: point resolution = 117 × 117 μm, section thickness = 2.0 mm, TR = 500 ms, TE = 2.497 ms, number of acquisitions = 8.

Examination of HER2/*neu* Expression Levels through Reverse Transcription−Polymerase Chain Reaction (RT−PCR) Analyses. HER2/*neu* mRNA expression of the cell lines used for in vitro cell studies was detected by RT−PCR analyses. HER2/*neu* mRNA was isolated from the cell lines by treating them with TRIzol and then transcripted reversely. The reversely transcripted products were amplified by PCR and analyzed by agarose gel electrophoresis. GADPH was used as an internal control. As shown in Supporting Figure 1, the fluorescence intensity of the HER2/*neu* gene gradually increases from Bx-PC-3 (a) to MDA-MB-231 (b), BT-474 (c), and NIH3T6.7 (d) cell lines.

Results and Discussion

Before one can utilize magnetic nanocrystals for MR signal enhancement, it is important to develop well-defined magnetic nanocrystals. The key requirement for this model system is the fabrication of high-quality magnetic nanocrystals in terms of the size, crystalline phase, and stoichiometry since these characteristics can affect the MR signals. Since conventional water phase synthetic protocols result in rather poor crystallinity and a large size distribution,[21] we instead utilized a high-temperature method where magnetic nanocrystals were synthesized through thermal decomposition of $Fe(acac)_3$ (acac = acetylacetonate) in a hot organic solvent.[20] Obtained nanocrystals are highly single-phased crystalline stoichiometric 9 nm Fe_3O_4 with a narrow size distribution (σ = ∼5%) (Figure 1a). The

(13) Josephson, L.; Tung, C. H.; Moore, A.; Weissleder, R. *Bioconjugate Chem.* **1999**, *10*, 186−191.
(14) Song, H.-T.; Choi, J.-s.; Huh, Y.-M.; Kim, S. J.; Jun, Y.-w.; Suh, J.-S.; Cheon, J. *J. Am. Chem. Soc.* **2005**, *127*, 9992−9993.
(15) Kang, H. W.; Josephson, L.; Petrovsky, A.; Weissleder, R.; Bogdanov, A., Jr. *Bioconjugate Chem.* **2002**, *13*, 122−127.
(16) Artemov, D.; Mori, N.; Okollie, B.; Bhujwalla, A. M. *Magn. Reson. Med.* **2003**, *49*, 403−408.
(17) Weissleder, R.; Moore, A.; Mahmood, U.; Bhorade, R.; Benveniste, H.; Chiocca, E. A.; Basilion, J. P. *Nat. Med.* **2000**, *6*, 351−355.
(18) Zhao, M.; Beauregard, D. A.; Loizou, L.; Davletov, B.; Brindle,K. M. *Nat. Med.* **2001**, *7*, 1241−1244.
(19) Jun, Y.; Huh, Y.-M.; Choi, J.; Lee, J.-H.; Song, H.-T.; Kim, S.; Yoon, S.; Kim, K.-S.; Shin, J.-S.; Suh, J.-S.; Cheon, J. *J. Am. Chem. Soc.* **2005**, *127*, 5732.
(20) Sun, S.; Zeng, H.; Robinson, D. B.; Raoux, S.; Rice, P. M.; Wang, S. X.; Li, G. *J. Am. Chem. Soc.* **2004**, *126*, 273−279.
(21) Sjögren, C. E.; Johansson, C.; Nævestad, A.; Sontum, P. C.; Briley-Sæbø, K.; Fahlvik, A. K. *Magn. Reson. Imaging* **1997**, *15*, 55−67.

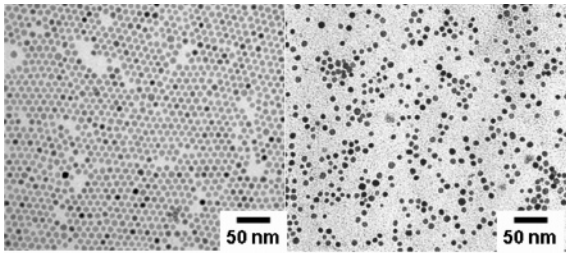

Figure 1. Transmission electron micrograph (TEM) of 9 nm iron oxide nanocrystals. (a) As-synthesized nanocrystals, (b) WSIO nanocrystals.

nanocrystals exhibit highly enhanced magnetic properties with the mass magnetization value of ∼80 emu/(g of Fe) compared to conventional iron-oxide-based MR signal enhancers.[19] Such enhanced magnetic properties of the magnetic nanocrystals result in significant improvement of MR contrast effect. T2-weighted MRI signal of a WSIO nanocrystal is ∼2.5 times larger than that of previously known cross-linked iron oxide (CLIO) signal enhancers[15,17] (see Supporting Information).

These nanocrystals are coated with oleic acid and oleylamine and are, therefore, insoluble in water. To make them water-soluble and biocompatible, a simple but highly effective 2,3-dimercaptosuccinic acid (DMSA) ligand was introduced onto the nanocrystal surface through simple mixing of the nanocrystals with a large excess of DMSA.[19] The DMSA binds to the iron oxide nanocrystal surface through its carboxylic bonding, and the intermolecular disulfide cross-linking between surface-bound DMSA ligands strengthens the nanocrystal stability. The remaining free carboxylic acid and thiol groups make the nanocrystals hydrophilic and are used for further conjugation of target-specific antibody. The DMSA-coated Fe_3O_4 nanocrystals are fairly stable in water and phosphate-buffered saline (PBS) without any aggregation. In TEM images of DMSA-coated Fe_3O_4 nanocrystals, presented in Figure 1b, the nanocrystals retain their original size of ∼9 nm without aggregation. Dynamic light scattering (DLS) measurement of the nanocrystals also confirms that the nanocrystals are highly monodisperse in water with the mean size of ∼9 nm, which is consistent with that observed by TEM analysis (Figure 2a). These nanocrystals are stable up to 250 mM NaCl solution and between pH 6 and 10. Since our magnetic nanocrystals contain much smaller ligands (DMSA, MW = 182) than previously observed for well-known large ligand systems, such as dextran (MW = 10 000−100 000), it is advantageous especially under in vivo conditions. Retaining the small probe size has been known to be critical for successful in vivo applications since large-sized probes significantly reduce their biostability, diffusion, and circulation processes, as well as increase undesired nonspecific binding and RES uptake.[22] Also, smaller-sized probes render enhanced biological targeting efficiency and specificity.[23]

Since our water-soluble iron oxide nanocrystals possess high monodispersity and stability in an aqueous media with enhanced magnetic property, we further examined their applicability for the in vitro and in vivo cancer diagnosis by conjugation of WSIO nanocrystals with a cancer-targeting antibody. As a possible model system, we chose Herceptin as the targeting antibody, which is a well-known antibody with specific binding ability

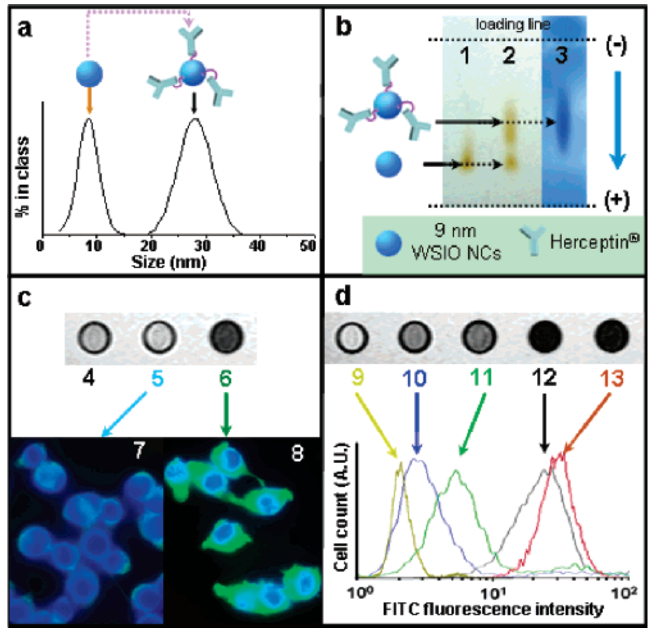

Figure 2. Formation of WSIO nanocrystals−Herceptin conjugates and in vitro evaluation of their binding specificity to HER2/*neu* cancer markers. (a) Dynamic light scattering (DLS) of 9 nm WSIO nanocrystals and WSIO−Herceptin conjugates. DLS data indicate 9 nm WSIO nanocrystals still retain their original size in aqueous phase, and the WSIO nanocrystals become ∼28 nm after Herceptin conjugation. (b) Gel electrophoresis of WSIO nanocrystals and WSIO−Herceptin conjugates. Analyses before (1) and after (2) Herceptin conjugation to WSIO nanocrystals show a new band with high retention time matched with protein staining test (3). (c) MR and optical imaging of nontreated (4), WSIO-irrelevant antibody control conjugate treated (5 and 7), and WSIO−Herceptin conjugate treated (6 and 8) fibroblast cell lines (NIH3T6.7) with HER2/*neu* cancer markers. In the MR images, while no noticeable difference is observed for the nontreated (4) and control conjugate treated (5) cells, significant darkening is evident for WSIO−Herceptin probe conjugates (6). Immunostaining test with FITC−anti-human IgG shows consistency with the MRI results. While no green fluorescence activity is seen from the control conjugate treated cells (7), vivid green fluorescence (8) indicative of successful receptor targeting from FITC is detected for WSIO−Herceptin probe conjugate treated cells. Blue fluorescence is from cell nuclei staining. (d) MR images and FACS analyses of WSIO−Herceptin probe conjugate treated cell lines with increasing expression levels of HER2/*neu* receptors: Bx-PC-3 (10), MDA-MB-231 (11), BT-474 (12), and NIH3T6.7 (13) cell lines. Control conjugates (9) are treated to Bx-PC-3 cell lines.

against a HER2/*neu* receptor overexpressed from breast cancer cells.[24] Previously, MR detection of HER2/*neu* receptor expression of in vitro cell lines has been reported,[16] where the detection system is based on the indirect imaging through the biotinylated Herceptin, which is already bound to the HER2/*neu* receptor. As a note, there has been no direct in vivo cancer targeting and imaging of HER2/*neu* with magnetic nanocrystal probes so far.

Conjugation of the WSIO nanocrystals with Herceptin was performed through a known sulfo-SMCC (sulfosuccinimidyl-4-(maleimidomethyl)cyclohexane-1-carboxylate) cross-linking procedure[25] and further verified by DLS measurements and gel electrophoresis (Figure 2a,b). Our WSIO−Herceptin probe conjugates have a hydrodynamic radius of around 14 nm, which is similar in size to those of previously reported quantum dot conjugates used for in vivo targeting experiments.[11]

We first examined in vitro binding specificity and efficiency by treating them to a fibroblast cell line, NIH3T6.7, which

(22) Pouliquen, D.; Le Jeune, J. J.; Perdrisot, R.; Ermias, A.; Jallet, P. *Magn. Reson. Imaging* **1991**, *9*, 275−283.
(23) Yokoyama, M.; Satoh, A.; Sakurai, A.; Okano, T.; Matsumura, Y.; Kakizoe, T.; Kataoka, K. *J. Control. Release* **1998**, *55*, 219−229.
(24) Hudziak, R. M.; Lewis, G. D.; Winget, M.; Fendly, B. M.; Shepard, H. M.; Ullrich, A. *Mol. Cell Biol.* **1989**, *9*, 1165−1172.
(25) Hermanson, G. T. *Bioconjugate Techniques*; Academic Press, Inc.: New York, 1996; pp 235−237.

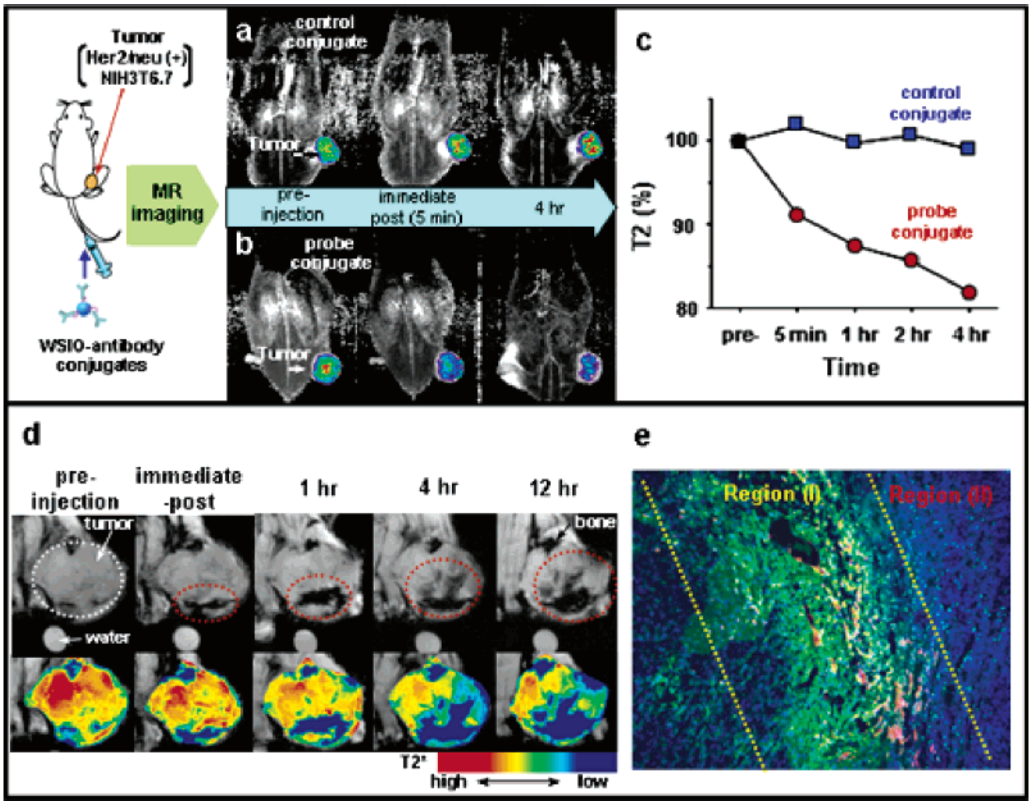

Figure 3. In vivo MRI of cancer-targeting events of WSIO−antibody conjugates. (a and b) Color maps of T2-weighted MR images of cancer cell implanted (NIH3T6.7) mice at the different temporal points (preinjection, immediate post, 4 h) after the intravenous injection of WSIO-irrelevant antibody control conjugates (a) and WSIO−Herceptin probe conjugates (b). Whereas no difference is seen in the color-mapped MRI for the control conjugate (a), an immediate (5 min) color change to blue at the tumor site is evident with the probe conjugate (b). (c) Plot of T2 values versus time after the injection of WSIO−antibody conjugates in (a) and (b) samples. (d) T2*-weighted MR images of cancer cell implanted (NIH3T6.7) mouse at 9.4 T and their color maps at different temporal points after probe conjugate injection. Tumor area is circled with white dotted lines. Dark MR image (red dotted circle) immediately appears near the bottom region of the tumor and then gradually diffuses to the central and upper region of the tumor. Color mapping of the identical MR images shows more details of MR signal changes. Progressive diffusion and targeting events of the probe conjugates (blue and green color) into tumor tissue are clearly observed with its increased occupation of roughly 1/3, 1/2, and 2/3 of tumor tissues at 1, 4, and 12 h, respectively. (e) Fluorescence immunohistochemical analyses of an excised tumor slice. Endothelial vessels were stained with rhodamine−anti-CD31 (red fluorescence), and probe conjugates were stained with FITC−anti-human IgG (green fluorescence). These fluorescence data indicate the presence of WSIO−Herceptin probe conjugates near the highly vascular region I of the tumor tissue. Blue background fluorescence (cell nuclei stained with DAPI) is observed at low vascular region II.

possesses overexpressed HER2/*neu* cancer markers. In the T2-weighted spin−echo MR images, no significant difference is observed between the nontreated (Figure 2c (4)) and WSIO-irrelevant antibody (anti-HMEN-B3) control conjugate treated cells (Figure 2c (5)). In contrast, the use of WSIO−Herceptin probe conjugates results in the significant darkening of MR images (Figure 2c (6)), which indicates selective binding of the probe conjugates to the target cells. This MRI result is also confirmed by an optical technique where an immunostaining test is performed by treating the cells with a secondary antibody of anti-human IgG labeled with fluorescein (FITC). While control conjugate treated cells do not show green fluorescence activity (Figure 2c (7)), vivid green fluorescence from the FITC is clearly observed for WSIO−Herceptin probe conjugates (Figure 2c (8)).

The relationship between MR signals and the binding activity of the WSIO−Herceptin probe conjugates was further examined for various cell lines with different levels of HER2/*neu* receptor expression: Bx-PC-3, MDA-MB-231, BT-474, and NIH3T6.7 cell lines, which are arranged in the order of increasing HER2/*neu* expression level. T2-weighted MR signals of the cell lines treated with WSIO−Herceptin probe conjugates become darker as the expression level of the HER2/*neu* receptors is increased (Figure 2d (10−13)). It is noteworthy that the MR signal intensities of the cell lines treated with WSIO−Herceptin probe conjugates show a marked difference from that of control conjugates (Figure 2d (9)), indicating excellent specific binding efficiency of the probe conjugates, even in the case of Bx-PC-3 cell lines with minimal expression of the receptors. These MR imaging results are also consistent with optical analyses where fluorescence-activated cell sorting (FACS) data show a continuous increase of FITC fluorescence intensity according to the order of the expression level of HER2/*neu* receptors (Figure 2d).

On the basis of our successful verification of WSIO−Herceptin probe conjugates for in vitro HER2/*neu* targeted MR imaging, we further tested their capability for in vivo use. A set of nude mouse subjects ($n = 8$) was implanted at their proximal thigh region with NIH3T6.7 cell lines overexpressed with HER2/*neu* cancer markers. MR imaging of the mice was performed at the different temporal points (e.g., preinjection, immediate post (~5 min), and 4 h) after the intravenous tail injection of WSIO−antibody conjugates (400 μg of Fe). In the control experiment with WSIO-irrelevant antibody conjugates, no change in the color-mapped MR signal (Figure 3a) and T2 values (Figure 3c) at the tumor site is observed. This is consistent with our in vitro studies and confirms minimal nonspecific binding to the tumor site. In contrast, after the injection of WSIO−Herceptin probe conjugates, immediate color change to blue is evident within 5 min, and a continuous T2 value drop of ∼10% is observed within 5 min and ∼20% at 4 h (Figure 3b,c). These results imply that the WSIO−Herceptin probe conjugates successfully reach and bind to the target cancer cells at the proximal thigh.

In addition to such static detection of cancer cells, our WSIO−Herceptin probe conjugates were used to monitor their progressive targeting events in vivo at higher magnetic fields (9.4 T). In 5 min, after the injection of WSIO−Herceptin probe conjugates into another mouse sample, a dark MR image appears near the bottom region of the tumor (red circle of Figure 3d, top) and then gradually grows and spreads to the central and upper region of the tumor as time durations of 1, 4, and 12 h. Color mapping of the identical MR images shows more details of MR signal changes (Figure 3d, bottom). Blue and green regions (corresponding to darker MR image or low T2* value) formed just after the injection expand horizontally and later move vertically as time goes with its increased occupation of roughly 1/3, 1/2, and 2/3 of tumor tissues at 1, 4, and 12 h, respectively, while yellow and red (corresponding to lighter MR image or high T2* value) regions gradually disappear. Presumably, this time-dependent MR signal change is related to the heterogeneous pattern of the intratumoral vasculature.[26] Fluorescence immunohistochemical studies of an excised tumor slice show that the distribution of WSIO−Herceptin probe conjugates (stained as green fluorescence) is localized around the highly vascular region where endothelial cells are stained as red fluorescence (Figure 3e, region I). In contrast, the blue background fluorescence (cell nuclei stained with DAPI) is observed in the low vascular region where no endothelial cells are stained (Figure 3e, region II). Since neovasculatures of a tumor generally have a leaky and porous structure, WSIO−Herceptin probe conjugates are easily permeable for more active targeting toward cancer cells in the highly vascular region of the tumor. Afterward, the probe conjugates could also gradually reach and accumulate to the less vascular region of the tumor as time elapses since unbound WSIO−Herceptin probes continuously recirculate in the blood and target cancer cells.

Conclusion

In summary, we present the development of a highly efficient and cancer-specific magnetic nanocrystal probe system for in vivo MR diagnosis of cancer. Well-defined material properties, such as small size, improved magnetism, high biostability, and also targeting moiety, are critical for the target-selective in vivo cancer detections. The protocols and iron oxide nanocrystal probe developed here can be applied for in vitro and in vivo MRI diagnosis for various types of cancer and can possibly be extended for other biomedical detections and applications.

Acknowledgment. We would like to thank Prof. S. Y. Kim, Prof. K.-H. Kim, and Dr. E. Scher for their insightful discussions and support, Dr. I.-G. Ko and S.-J. Ko for assistance with the in vitro cell studies, I. H. Park for antibody purification, K. T. Son (KBSI-Chuncheon) for TEM, Dr. Y. J. Kim (KBSI) for HVEM, Dr. O.-H. Han (KBSI-Daegu) for NMR, and Dr. S. J. Oh (KBSI) for SQUID. This work is supported by the Korea Research Foundation (R02-2004-000-10096-0).

Supporting Information Available: The examination of HER2/*neu* receptor expression, cytotoxicity profile of WSIO, T2 relaxivity of WSIO and CLIO, magnetic properties of 9 nm iron oxide nanocrystals, and complete ref 12. This material is available free of charge via the Internet at http://pubs.acs.org.

JA052337C

(26) Weidner, N.; Semple, J. P.; Welch, W. R.; Folkman, J. *N. Engl. J. Med.* **1991**, *324*, 1−8.